Available online at www.sciencedirect.com

ScienceDirect

journal homepage: www.elsevier.com/locate/he

Protonic and electronic conductivity of the layered perovskite oxides $HCa_2Nb_3O_{10}$ and $Ca_4Nb_6O_{19}$

Thomas I. Draskovic [1], *TsingHai Wang* [2], *Camden N. Henderson*, *Thomas E. Mallouk**

Department of Chemistry, The Pennsylvania State University, University Park, PA 16802, USA

ARTICLE INFO

Article history:
Received 24 December 2013
Received in revised form
30 December 2013
Accepted 4 January 2014
Available online 1 February 2014

Keywords:
Layer perovskite
Solid electrolyte
Mixed valence
Electronic conductivity
Intermediate temperature fuel cell

ABSTRACT

The structural and electrical properties of the Dion–Jacobson series layer perovskite $HCa_2Nb_3O_{10}$ were investigated. Within the intermediate temperature range (200–475 °C), the compound undergoes topochemical dehydration to $Ca_4Nb_6O_{19}$ and, under reducing atmospheres, partial reduction of Nb(V) to Nb(IV). These changes occur upon heating and are not reversed on cooling. Analysis of impedance data shows that the conductivity of $Ca_4Nb_6O_{19}$ is predominantly electronic under reducing atmospheres, consistent with the behavior of other structurally related mixed-valence layered niobates.

1. Introduction

Intermediate temperature proton conductors are of interest for possible applications in all-inorganic fuel cells. Compared to low temperature polymer electrolyte fuel cells and high temperature solid oxide fuel cells (SOFC), fuel cells that operate in the intermediate temperature range (~200–450 °C) offer several advantages, such as greater immunity to catalyst poisoning, higher catalyst activity, and fewer engineering issues stemming from the high temperature of operation of SOFCs. Perovskite oxides are often used as oxide ion conductors in SOFCs and have been the focus of much research on intermediate temperature proton conductors [1–3]. Recently, Pergolesi et al. reported that thin films of the anion-defective perovskite $BaZr_{0.8}Y_{0.2}O_{3-\delta}$ have a conductivity of 0.11 Ω^{-1} cm^{-1} at 500 °C [4]. In principle, thin films of such electronically insulating proton conductors on hydrogen-permeable metallic foils [5–7] could serve as low resistance membranes for intermediate temperature fuel cells.

Many of the best intermediate temperature proton conductors are perovskites that contain defects on oxygen atom sites in the lattice [8]. Layer perovskites are intergrowths of the ABO_3 perovskite structure with other metal oxide

Abbreviations: XRD, X-ray powder diffraction; SOFC, solid oxide fuel cell.

* *Corresponding author*. Tel.: +1 814 863 9637; fax: +1 814 865 2925.
E-mail address: tem5@psu.edu (T.E. Mallouk).

[1] Present address: Department of Chemistry and Biochemistry, The Ohio State University, Columbus, OH 43210, USA.
[2] Present address: Nuclear Science and Technology Development Center, National TsingHua University, Hsinchu 300, Taiwan.

0360-3199/$ – see front matter
http://dx.doi.org/10.1016/j.ijhydene.2014.01.017

structures. Compounds in the Ruddlesden-Popper ($A'_2[A_{n-1}B_nO_{3n+1}]$) [9,10] and Dion–Jacobson series ($A'[A_{n-1}B_nO_{3n+1}]$, A′ = alkali metal) [14–16], can undergo intercalation, ion exchange, exfoliation, and condensation reactions, which provide synthetic routes to unique ceramic materials and thin films. The structural and electrical properties of the three-layer Dion–Jacobson phase compounds $A'[Ca_2Nb_3O_{10}]$ (A′ = K, Rb, Cs) and their proton-exchanged derivatives have been studied since their discovery in the early 1980s [11–18]. Early investigations by Thangadurai et al. into the potential proton conductivity of $HCa_2Nb_3O_{10}$ were promising, as high conductivity (10^{-4}–$10^{-3}\ \Omega^{-1}\ cm^{-1}$) was observed below 450 °C [15]. Although protonic conduction was proposed as the dominant transport mechanism, the exact origins of the high conductivity were not clearly established. We subsequently observed that the structurally similar two-layer Dion–Jacobson phase niobate $HLaNb_2O_7\cdot 0.5H_2O$ underwent partial reduction in wet or dry hydrogen atmospheres [19]. In this compound and the related two-layer Dion Jacobson oxyfluoride $H_{1-x}Rb_xLaNb_2O_6F$, impedance measurements established that the conductivity is predominantly electronic [20]. This has prompted us to re-examine the conductivity of $HCa_2Nb_3O_{10}$ and its lamellar intermediate temperature condensation product $Ca_4Nb_6O_{19}$ in oxidizing and reducing atmospheres, to address the question of the potential utility of layer perovskite niobates as proton conductors for intermediate temperature fuel cells and related applications.

2. Experimental section

2.1. Synthesis and proton exchange of $KCa_2Nb_3O_{10}$

The Dion–Jacobson compound $KCa_2Nb_3O_{10}$ was prepared by grinding together K_2CO_3 (Aldrich, 99+%) (20% excess), $CaCO_3$ (Aldrich, 99.995+%), and Nb_2O_5 (Aldrich, 99.99%) and firing the mixture in air at 1100 °C for 24 h [5]. Proton exchange of the $KCa_2Nb_3O_{10}$ product was carried out by constant shaking at room temperature, using an excess of nitric acid (1 M) for at least 3 days with daily centrifugation and replacement of the acid solution. The product was isolated by centrifugation, washing, and drying at 60 °C under reduced pressure. The identity and purity of the product phases were confirmed by X-ray powder diffraction (XRD).

2.2. Structural characterization and impedance measurements

XRD patterns were obtained using a Philips X'Pert MPD diffractometer with monochromatized Cu Kα radiation.

Pelleted samples of $HCa_2Nb_3O_{10}\cdot 0.5H_2O$ were prepared by pressing 0.5 g of powder in a cylindrical die at 3 metric tons, yielding pellets 13 mm in diameter and typically 1 mm thick. Pellets were coated on both sides with 100 nm thick films of Pt by sputtering to produce circular contacts. Because $HCa_2Nb_3O_{10}\cdot 0.5H_2O$ loses its water of hydration below 200°, the compound is formulated in the discussion below as $HCa_2Nb_3O_{10}$ at the start of the impedance measurements, which were carried out between 200 and 475 °C. Two-point impedance measurements were obtained using a Solartron 1255B Frequency Response Analyzer with a Solartron 1287 Electrochemical Interface, zero DC bias, and an AC voltage amplitude of 100 mV. Maximum frequencies ranged from 1 MHz to 5 mHz, depending on the sample. Subsequent heating and cooling cycles were performed, allowing for sample equilibration at each temperature in the range 200–475 °C. Measurements were conducted under humidified air and humidified H_2 (5%, balance Ar) atmospheres, produced

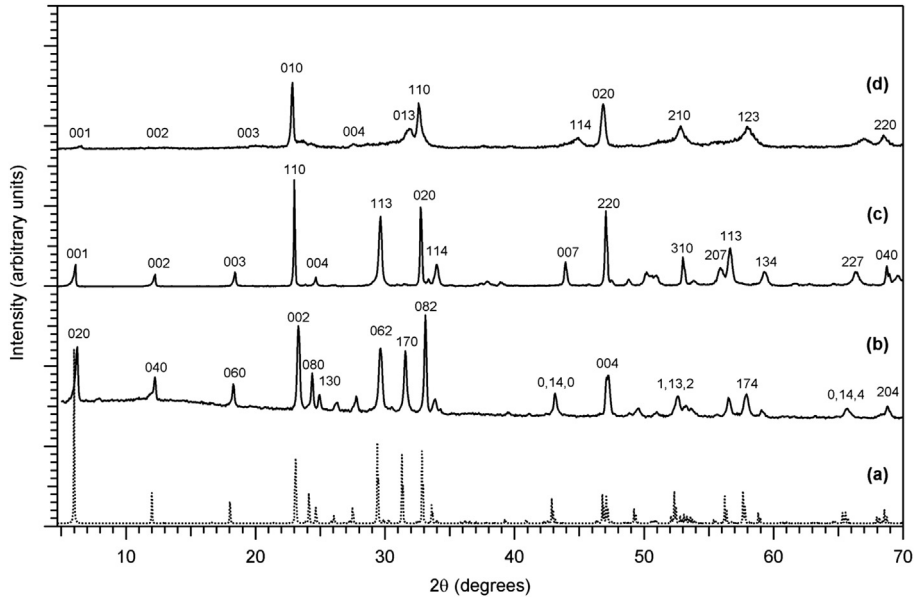

Fig. 1 – (a) Simulated and (b) experimental X-ray powder diffraction patterns of $KCa_2Nb_3O_{10}$ (indexed in space group Cmcm, a = 3.858(9) A, b = 29.36(6), c = 7.708(13) A), (c) its proton-exchanged derivative $HCa_2Nb_3O_{10}\cdot 0.5H_2O$ (P4/mbm, a = 5.461, c = 14.424 A), and (d) the dehydration product $Ca_4Nb_6O_{19}$ (P4/mmm, a = 3.846, c = 12.611 A).

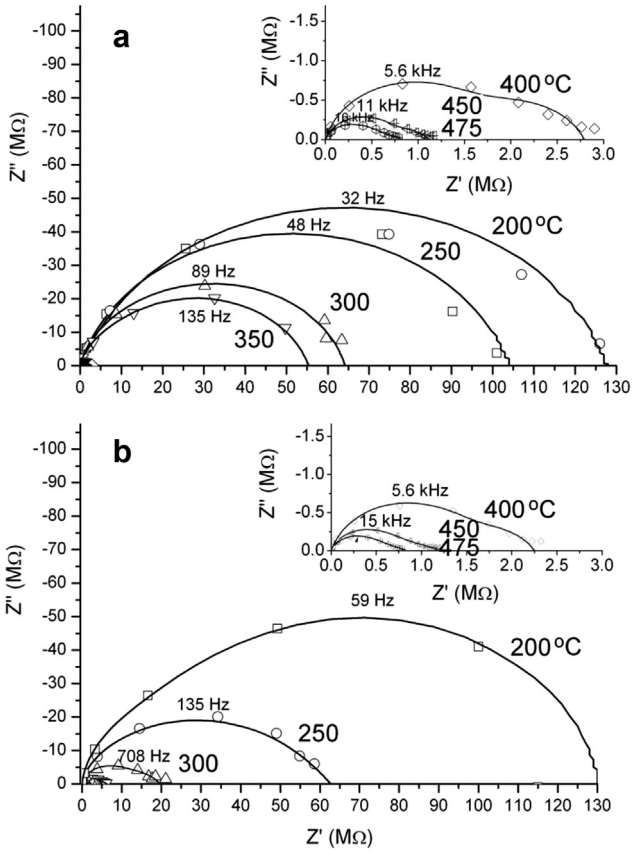

Fig. 2 – Impedance spectra of $HCa_2Nb_3O_{10}$ recorded at 200–475 °C in humidified air (P_{H_2O} = 23 torr) upon heating (a) and cooling (b). Inset graphs show an expanded view of the higher temperature data near the origin of the plot. The solid lines represent fits to the equivalent circuit shown in Fig. 4. Frequency increases from right to left along each curve, and the frequency at the top of each curve is indicated in the plot.

by bubbling the carrier gas through water at 25 °C (P_{H_2O} = 23 torr).

3. Results and discussion

3.1. *Dehydration and reduction of $HCa_2Nb_3O_{10}\cdot 0.5H_2O$ under reducing atmospheres*

X-ray diffraction patterns of $KCa_2Nb_3O_{10}$ and its proton-exchanged derivative $HCa_2Nb_3O_{10}\cdot 0.5H_2O$ were in agreement with prior literature reports [11–13,21]. Previous studies on $HCa_2Nb_3O_{10}$ have shown that upon heating above 300 °C, a metastable dehydration product $Ca_4Nb_6O_{19}$ is formed by topochemical collapse of the interlayer galleries [16]. In addition, it is known that Nb(V) in the Dion–Jacobson series $AA'_{n-1}Nb_nO_{3n+1}$ can be partially reduced to Nb(IV) by heating in a H_2 atmosphere [17–19,22]. The reduced niobium is relatively stable towards oxidation in air and has little effect on the lattice structure. Exposure of a $HCa_2Nb_3O_{10}.0.5H_2O$ sample to dry H_2 (5%, balance Ar) for 3 h at 450 °C was performed to confirm that dehydration and reduction could occur in the intermediate temperature range of interest. The powder sample changed from white to bluish gray in color and XRD analysis gave a diffraction pattern consistent with that of $Ca_4Nb_6O_{19}$ (Fig. 1). The change in color can be attributed to partial reduction of niobium and the likely formation of a mixed valence state. This color change was retained upon cooling to ambient temperature in the same gas mixture.

These reactions in the intermediate temperature range are problematic for applications as solid electrolytes, because mixed valent niobates are typically electronic conductors. The metastable $Ca_4Nb_6O_{19}$ is semiconducting and has higher electronic conductivity than the parent compound $HCa_2Nb_3O_{10}$ [16].

3.2. *Impedance measurements in humidified air and hydrogen*

Previous studies have established that the introduction of water can suppress the reduction of Nb(V) to Nb(IV) in layer perovskites [19]. Under humidified hydrogen, the equilibrium pO_2 is orders of magnitude higher than under dry hydrogen. Accordingly, experiments were done under humidified conditions. Impedance spectra of $HCa_2Nb_3O_{10}$ recorded in humidified air and H_2 atmospheres are shown in Figs. 2 and 3, respectively. A previously developed brick-layer model [23], which includes both grain and grain boundary conduction pathways, was used to analyze the data. The equivalent circuit in this model is shown in Fig. 4. Because the ionic and electronic conductivity act in parallel within the crystal grains, they are represented together as $R_{series} = (1/R_{elec} + 1/R_{ionic})^{-1}$. The charge transfer resistance (R_{ct}) represents the real part of the impedance at the grain boundaries. Fits of the impedance data improve when cell and grain boundary capacitances are replaced by constant phase elements (CPE). In

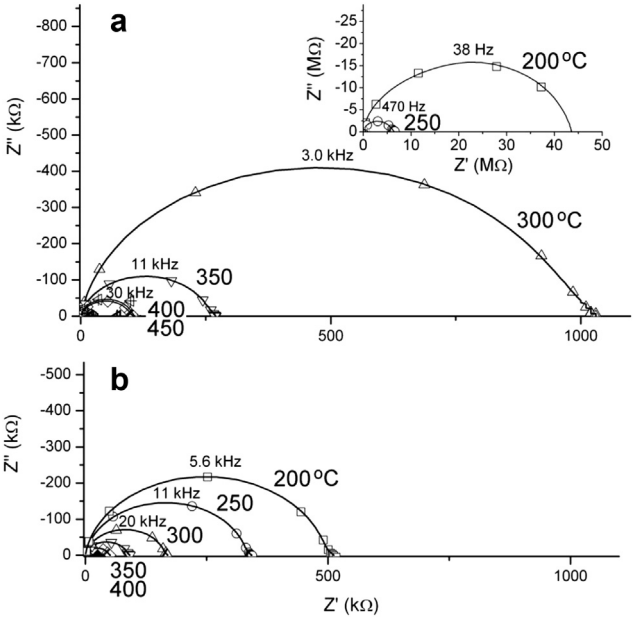

Fig. 3 – Impedance spectra of $HCa_2Nb_3O_{10}$ recorded in humidified 5% hydrogen (P_{H_2O} = 23 torr) upon heating (a) and cooling (b).

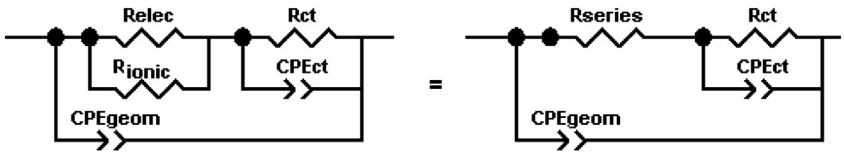

Fig. 4 – Equivalent circuit used to fit the impedance data.

this case, R_{series} and R_{ct} no longer correspond strictly to grain and grain boundary values, but their series combination still represents the low frequency impedance of the circuit.

When $HCa_2Nb_3O_{10}$ is heated in an atmosphere of humidified air, both the series component of the resistance R_{series} and the charge transfer resistance R_{ct} decrease with increasing temperature. Nyquist plots recorded between 200 and 475 °C (Fig. 2) are strikingly similar in the heating and cooling directions. At 200 °C, R_{series} and R_{ct} are both in the range of 10^8 Ω and drop to ~10^6 Ω upon heating to 475 °C. At the lower end of the temperature range, only one semicircle can be resolved in the Nyquist plots, but at higher temperature, where R_{ct} exceeds R_{series}, a second low-frequency semicircle begins to emerge. These changes in impedance are consistent with an activated conduction process, but they do not differentiate between electronic hopping conduction and protonic conduction.

Under humidified hydrogen, the impedance behavior of $HCa_2Nb_3O_{10}$ is quite different. Fig. 3 shows Nyquist plots recorded upon heating and cooling. Initially, at 200 °C, the values of R_{ct} and R_{series} are slightly lower (by a factor of ~2) than they are in humidified air. As the temperature is increased, R_{ct} and R_{series} drop by four and three orders of magnitude, respectively. In contrast to the behavior in humidified air, cooling from 475 to 200 °C results in an increase of only one order of magnitude in both R_{ct} and R_{series}.

These features in the impedance spectra can be rationalized in terms of the known phase behavior of $HCa_2Nb_3O_{10}$. In the heating part of the cycle, $HCa_2Nb_3O_{10}$ undergoes irreversible dehydration to $Ca_4Nb_6O_{19}$. The changes in R_{series} and R_{ct} upon heating and cooling in air are consistent with thermally activated electronic conductivity of semiconducting $Ca_4Nb_6O_{19}$, and/or with thermally activated proton conductivity. The more pronounced drop in resistance under humid hydrogen can be interpreted as arising from partial reduction of Nb(V) to form a mixed-valent electronic conductor. This material remains partially reduced (and therefore electronically conducting) as the temperature is lowered under the H_2 atmosphere.

Total conductances of the samples were obtained by fitting the impedance data shown in Figs. 2 and 3 to the equivalent circuit in Fig. 4. The total impedance in the low frequency limit corresponds to the sum of the series and charge transfer resistances, $R_{total} = R_{series} + R_{ct}$. The values of R_{total} obtained in this way were, as expected, very close to the Z′-axis intercepts of the Nyquist shown in Figs. 2 and 3. The corresponding total conductivity values are plotted as a function of temperature and atmosphere in Fig. 5. In air during the heating part of the cycle, the conductivity remains fairly constant until 350 °C. Below this temperature, protonic conductivity is likely the dominant transport mechanism [19]. Mobile protons are created by hydration of oxide ion vacancies, according to the following mechanism:

$$H_2O(g) + v_o^{\cdot\cdot} + O_o^x = 2OH_o^{\cdot} \quad (1)$$

Above 350 °C, there is a sharp jump in conductivity as the material dehydrates to the semiconducting $Ca_4Nb_6O_{19}$ phase. Past this point, the conductivity follows an Arrhenius relation with an apparent activation energy of 0.59 ± 0.03 eV on the subsequent cooling cycle. In the reducing hydrogen atmosphere, the initial conductivity is close to that in humidified air. However there is a more rapid increase upon heating between 200 and 350 °C, consistent with reduction of Nb(V) to Nb(IV), which occurs prior to the phase transition to $Ca_4Nb_6O_{19}$. The conductivity in the humid hydrogen atmosphere decreases upon cooling with an apparent activation energy of 0.35 ± 0.04 eV. Comparing the cooling cycles, the similar activation energies suggest that electronic hopping conduction dominates in both atmospheres. If this interpretation is correct, the different intercepts indicate a 20–30 fold increase in the density of charge carriers in a reducing atmosphere.

4. Conclusions

An early conductivity study of $HCa_2Nb_3O_{10}$ in hydrogen atmospheres suggested that the high conductivities observed were likely to be protonic in origin [15]. Reproducible conductivity measurements were presented from the second and

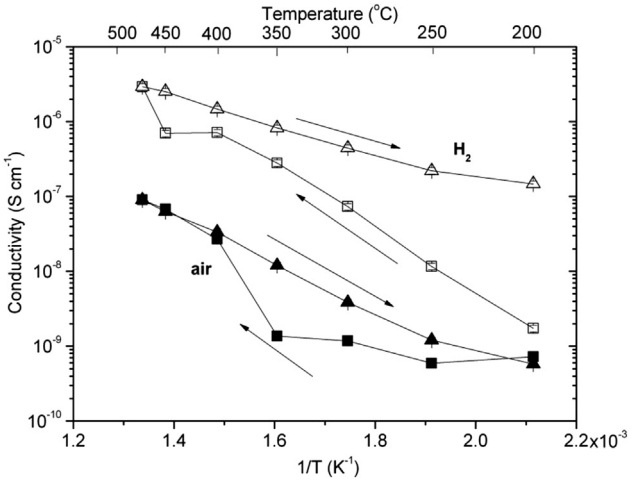

Fig. 5 – Conductivity vs. reciprocal temperature for $HCa_2Nb_3O_{10}$ in humidified air and hydrogen during heating cooling cycles. Error bars shown represent one standard deviation of the mean value.

subsequent heating/cooling cycles. The conductivity followed linear Arrhenius behavior, much like that observed after the initial heating cycle in our experiments. However that study was conducted before the phase transition from $HCa_2Nb_3O_{10}$ to $Ca_4Nb_6O_{19}$ had been characterized and also prior to much of the literature on the formation of mixed valent Nb(V/IV) compounds among Dion–Jacobson phase niobates. We conclude from this study that these niobates have significant electronic conductivity under intermediate temperature conditions, especially in reducing humid atmospheres, and thus they are unlikely to be useful as proton conductors in intermediate temperature fuel cells. It is important to note that isostructural Dion–Jacobson phase tantalates are known, and it is possible that some of those compounds will be less susceptible to reduction, and also may not undergo the same phase transition that eliminates mobile protons in $HCa_2Nb_3O_{10}$.

Acknowledgment

This work was supported by the National Science Foundation under grant CHE-0910513.

REFERENCES

[1] Takahashi T, Iwahara H. Solid state ionics – protonic conduction in perovskite-type oxide solid solutions. Rev Chim Min 1980;17:243–53.
[2] Kreuer KD. On the development of proton conducting materials for technological applications. Solid State Ionics 1997;97:1–15.
[3] Ma G, Shimura T, Iwahara H. Ionic conduction and nonstoichiometry in $Ba_xCe_{0.90}Y_{0.10}O_{3-\alpha}$. Solid State Ionics 1998;110:103–10.
[4] Pergolesi D, Fabbri E, D'Epifanio A, Bartolomeo ED, Tebano A, Sanna S, et al. High proton conduction in grain-boundary-free yttrium-doped barium zirconate films grown by pulsed laser deposition. Nat Mater 2010;9:846–52.
[5] Yamaguchi S, Shishido T, Yugami H, Yamamoto S, Hara S. Construction of fuel cells based on thin proton conducting oxide electrolyte and hydrogen-permeable metal membrane electrode. Solid State Ionics 2003;162:291–6.
[6] Ito N, Iijima M, Kimura K, Iguchi S. New intermediate temperature fuel cell with ultra-thin proton conductor electrolyte. J Power Sources 2005;152:200–3.
[7] Fan CQ, Rivera H, Rao U, Liu R, Smotkin ES. Applications of metal hydride-based bipolar electrodes. Electrochim Acta 2012;59:470–3.
[8] Norby T. Solid-state protonic conductors: principles, properties, progress and prospects. Solid State Ionics 1999;125:1–11.
[9] Ruddlesden SN, Popper P. New compounds of the K_2NiF_4 type. Acta Crystallogr 1957;10:538–9;
The compound $Sr_3Ti_2O_7$ and its structure. Acta Crystallogr 1958;11:54–5.
[10] Uma S, Raju AR, Gopalakrishnan J. Bridging the Ruddlesden–Popper and the Dion–Jacobson series of layered perovskites – synthesis of layered oxides, $A_{2-x}La_2Ti_{3-x}Nb_xO_{10}$ (A = K, Rb), exhibiting ion-exchange. J Mater Chem 1993;3:709–13.
[11] Dion M, Ganne M, Tournoux M. The new phase families $M_IM_2(II)Nb_30_{10}$ with perovskite sheets. Mater Res Bull 1981;16:1429–35.
[12] Jacobson AJ, Johnson JW, Lewandowski JT. Interlayer chemistry between thick transition-metal oxide layers - synthesis and intercalation reactions of $K[Ca_2Na_{n-3}Nb_nO_{3n+1}]$ ($3 < N < 7$). Inorg Chem 1985;24:3727–9.
[13] Treacy MMJ, Rice SB, Jacobson AJ, Lewandowski JT. Electron-microscopy study of delamination in dispersions of the perovskite-related layered phases $K[Ca_2Na_{n-3}Nb_nO_{3n+1}]$ – evidence for single-layer formation. Chem Mater 1990;2:279–86.
[14] Fukuoka H, Isami T, Yamanaka S. Crystal structure of a layered perovskite niobate $KCa_2Nb_3O_{10}$. J Solid State Chem 2000;151:40–5.
[15] Thangadurai V, Shukla AK, Gopalakrishnan J. Proton conduction in layered perovskite oxides. Solid State Ionics 1994;73:9–14.
[16] Fang M, Kim CH, Mallouk TE. Dielectric properties of the lamellar niobates and titanoniobates $AM_2Nb_3O_{10}$ and $ATiNbO_5$ (A = H, K, M = Ca, Pb), and their condensation products $Ca_4Nb_6O_{19}$ and $Ti_2Nb_2O_9$. Chem Mater 1999;11:1519–25.
[17] Gomez-Romero P, Palacin MR, Casan N, Fuertes A. Synthesis of a reduced niobium "blue" with a layered perovskite structure. Solid State Ionics 1993;63–64:424–8.
[18] Palacin MR, Lira M, Garcia JL, Caldes MT, Casan-Pastor N, Fuertes A, et al. Synthesis deintercalation and transport properties of a mixed-valence derivative of the layered oxide $HLaNb_2O_7$. Mater Res Bull 1996;31:217–25.
[19] Kobayashi Y, Schottenfeld JA, Macdonald DD, Mallouk TE. Structural effects in the protonic/electronic conductivity of Dion–Jacobson phase niobate and tantalate layered perovskites. J Phys Chem C 2007;111:3185–91.
[20] Kobayashi Y, Tian M, Eguchi M, Mallouk TE. Ion-exchangeable, electronically conducting layered perovskite oxyfluorides. J Am Chem Soc 2009;131:9849–55.
[21] Chen Y, Zhao X, Ma H, Ma S, Huang G, Makita Y, et al. Structure and dehydration of layered perovskite niobate with bilayer hydrates prepared by exfoliation/self-assembly process. J Solid State Chem 2008;181:1684–94.
[22] Hamada D, Machida M, Sugahara Y, Kuroda K. Preparation and electrical properties of $KCa_{2-x}La_xNb_3O_{10}$. J Mater Chem 1996;6:69–72.
[23] Haile SM, West D, Campbell J. The role of microstructure and processing on the proton conducting properties of gadolinium-doped barium cerate. J Mater Res 1998;13:1576–95.